INORGANIC CHEMISTRY
FRONTIERS

RESEARCH ARTICLE

View Article Online
View Journal | View Issue

Cite this: *Inorg. Chem. Front.*, 2023, **10**, 4881

A multifunctional molecular ferroelectric with a high Curie temperature and electrical–thermal double-switch coexistence: $(C_8H_{14}NO)[FeCl_4]$†

Fang-Xin Wang, Yun-Zhi Tang, * Yu-Hui Tan, * Yi-Ran Zhao, Jia-Ying Wang, Yu-Kong Li, Hao Zhang, Ting-Ting Ying and Ming-Yang Wan

Received 24th May 2023,
Accepted 12th July 2023

DOI: 10.1039/d3qi00964e

rsc.li/frontiers-inorganic

Quasi-spherical molecules are used to construct high-performance molecular ferroelectrics, but accurately producing polar crystals with low symmetry remains a challenge. Herein, we report a novel high-temperature multiaxial molecular ferroelectric $(C_8H_{14}NO)[FeCl_4]$ (**1**) ($C_8H_{14}NO$ = 1-methyl-3-quinuclidinol). Dielectric and differential scanning calorimetry (DSC) measurements showed that compound **1** had a high Curie temperature of 341.8 K. It crystallizes in the $Cmc2_1$ space group at room temperature, showing switchable SHG response, moderate spontaneous polarization (P_s = 0.24 μC cm^{-2}), and clear ferroelectric domains. In addition, DSC and dielectric cycling tests indicate that compound **1** can be used as an excellent electric double-switch material. Notably, the distinct symmetry breaking, that is, 4/*mmm*F*mm*2, leads to a biaxial ferroelectric with four equivalent directions of polarization. This discovery provides an effective approach for constructing multiaxial high-temperature molecular ferroelectrics.

Introduction

A ferroelectric material is a kind of crystalline material that has spontaneous polarization and reverses or reorients under an applied electric field.[1,2] It has important applications in data storage, sensors, photoelectric equipment and so on. Inorganic ferroelectric ceramics have been dominant in research for a long time because of their outstanding piezoelectric properties.[3,4] However, traditional ferroelectric ceramics have little mechanical flexibility and require high machining temperatures, and the increasing demand for flexible and thin-film integrated devices poses challenges to traditional ferroelectric ceramics.[5,6] Molecular ferroelectrics have made remarkable progress in recent years, becoming a promising complement to traditional inorganic ferroelectrics due to their advantages of structural tunability, low impedance, environmental friendliness, mechanical flexibility and ease of preparation.[7–9] Among them, organic–inorganic hybrid metal halide ferroelectrics have the advantages of both organic and inorganic parts. They have not only rich structural diversity, but also rich physical properties.[10–16] At present, they receive wide attention in the exploration of multi-ferroelectrics, semiconductors, photovoltaics and other ferroelectric based multifunctional materials.[17,18] The preparation of organic–inorganic hybrid metal halides using organic amines and metal halides is usually an effective strategy to obtain temperature-triggered phase change materials, the mechanism of which is usually the ordered and disordered motion of flexible organic cations.[19–21] However, the phase transition temperatures of most molecular ferroelectrics reported are very low, mostly around or even below room temperature, such as those of $(C_6H_5CH_2CH_2NH_3)_2[CdI_4]$ (T_c = 301 K),[22] $(CH_3)_3NHBr$ (T_c = 286 K),[23] $(DMA)_4[PbI_6]$ (T_c = 252 K),[24] and [(4-methoxyanilinium)(18-crown-6)][ReO_4] (T_c = 153 K),[25] and a small number of high temperature molecular ferroelectrics are affected by uniaxial properties, such as (3-pyrrolinium)[$MnCl_3$] (T_c = 376 K),[26] which seriously hinders their application potential. Thanks to the multiaxial nature their ferroelectric and piezoelectric properties can be optimized,[27] and it is important to explore molecular ferroelectrics with high Curie temperature and multiaxial properties.

Hybrid metal halides with spherical organic molecules, such as quinine, 1,4-diazocyclic [2.2.2] octane (dabco), and $(Me_4N)^+$, have low rotational energy barriers and can induce structural phase transitions. However, due to the high symmetry, these spherical molecules usually crystallize in the center symmetric space group. Xiong *et al.* proposed the "quasi-spherical theory",[28] that is, through modifying spherical molecules the symmetry of molecules can be reduced, in

Faculty of Materials Metallurgy and Chemistry, Jiangxi University of Science and Technology, Ganzhou 341000, Jiangxi Province, P.R. China.
E-mail: tangyunzhi75@163.com, tyxcn@163.com

†Electronic supplementary information (ESI) available: Additional data. CCDC 2243166. For ESI and crystallographic data in CIF or other electronic format see DOI: https://doi.org/10.1039/d3qi00964e

order to promote crystallization in the polar space group that is not highly symmetrical, which is beneficial for the ferroelectric behavior. Recently, quasi-spherical molecules have been used to construct high performance molecular ferroelectrics.[29–31] For example, the molecular modification of $(Me_4N)^+$ cations, by substituting a methyl group with chloromethyl, iodomethyl, and hydroxyl groups, can successfully reduce the symmetry of the molecule from point group T_d to C_{3v}. When these modified organic cations were assembled with anions, molecular ferroelectrics $(Me_3NCH_2Cl)[CdCl_3]$,[32] $(Me_3NCH_2I)[PbI_3]$,[33] and $(Me_3NOH)[KFe(CN)_6]$[34] were obtained successfully. Another example is the modification of dabco. A methyl group is added to an N atom to break the symmetry structure of dabco, thus reducing the molecular symmetry from D_{3h} to C_{3v}. (Mdabco)$[RbI_3]$[33] was obtained by assembling it with metal halides.

Based on the quasi-spherical theory, we used low symmetry 1-methyl-3-quininocyclone cations as polar components to prepare a new multifunctional organic–inorganic hybrid ferroelectric $(C_8H_{14}NO)[FeCl_4]$ (Scheme 1). It shows an obvious switchable nonlinear optical response, excellent ferroelectricity (T_c = 345 K and moderate spontaneous polarization P_s = 0.24 μC cm^{-2}) and clear ferroelectric domains. Specifically, **1** is a multiaxial ferroelectric (Aizu notation: 4/*mmmFmm*2). Therefore, the discovery of compound **1** enriches the high-temperature multiaxial organic–inorganic hybrid ferroelectric library, opening up the way for multifunctional ferroelectric applications.

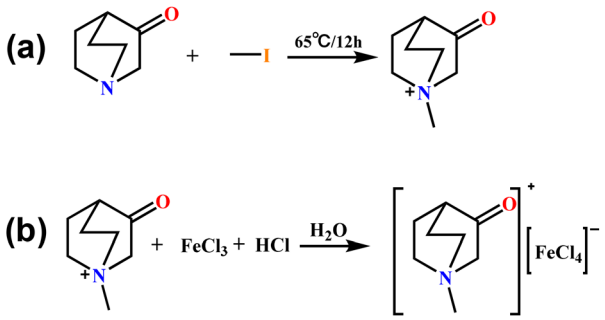

Scheme 1 (a) Synthesis flow chart of the organic cation $[C_8H_{14}NO]^+$. (b) Schematic diagram of the synthesis of compound **1**.

Results and discussion

Differential scanning calorimetry (DSC) and dielectric properties

In order to determine the existence of reversible structural phase transitions, the thermal anomalies of compound **1** during heating/cooling were tested by DSC in the temperature range of 318–358 K (Fig. 1a). The endothermic and exothermic peaks of compound **1** were 341.8 K and 328.7 K, respectively. In addition, the wide reversible peak and the thermal hysteresis of 13 K in the DSC curve are consistent with the characteristics of first-order phase transition.[35] We further calculated that the entropy changes (ΔS) of compound **1** during heating

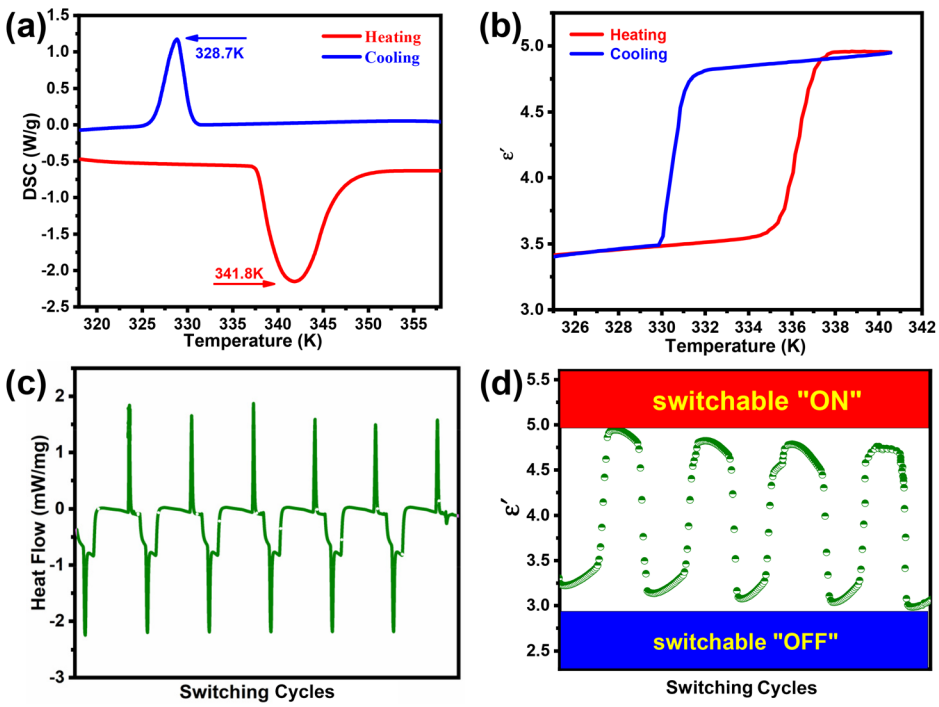

Fig. 1 DSC analysis (a); temperature dependence of the real part of the dielectric constant (b); DSC cycle test of compound **1** (c) with a scan rate of 10 K min^{-1}; and the dielectric switching cycle measurement of compound **1** (d).

and cooling are about 37.92 J mol^{-1} K^{-1} and 37.39 J mol^{-1} K^{-1}, respectively. According to the Boltzmann equation $\Delta S = nR \ln N$ (where N represents the possible orientation), the estimated N values of 95.679 and 89.747 are significantly greater than 1, and the ΔS and N obtained in both phases are roughly the same, suggesting that compound **1** undergoes a solid-state reversible phase transition. These high Curie temperatures, giant entropy changes and N values indicate that compound **1** has serious molecular disordered motion and structural deformation during the phase transition. In addition, we conducted DSC cycling tests on compound **1** using a scanning rate of 10 K min^{-1} (Fig. 1c). The test results indicate that even after 6 cycles of endothermic and exothermic cycles, the phase transition can still maintain its initial endothermic and exothermic effects. This indicates that compound **1** can be used as an excellent thermal switch material. The TG-DTA measurements (Fig. S2†) of compound **1** showed that the decomposition began at 573 K, which is much higher than the structural phase transition temperature (T_c = 341.8 K), indicating that compound **1** has good thermal stability.

The phase transition behavior of crystals is usually accompanied by dielectric anomalies. The dielectric behavior can be expressed by measuring the temperature dependence of the real part of the complex dielectric constant ε' (where $\varepsilon = \varepsilon' - i\varepsilon''$ is the complex electric permittivity). In general, once a structural phase transition occurs, it results in an abnormal transition from a low dielectric state to a high dielectric state.[36] In order to further confirm the structural phase transition of compound **1**, the dielectric properties of compound **1** were measured by pressing it into a sheet. As expected, the dielectric anomaly of compound **1** shows a perfect step shape near the phase transition temperature during heating and cooling, with the real part of the dielectric constant increasing sharply at 336 K when heating and decreasing sharply at 331 K when cooling (Fig. 1b). These results are consistent with those of DSC measurements. As shown in Fig. 1d, the dielectric switch of compound **1** showed no significant dielectric loss after four consecutive cycles, demonstrating significant reversible dielectric switching and fatigue resistance. In the dielectric cycling test, the low and high dielectric constant states are similar to "off" and "on", respectively.[37] This indicates that compound **1** can be used as an excellent electric switch material.

Crystal structure analysis

In order to reveal the ferroelectric transformation mechanism of compound **1**, the single crystal structure of compound **1** was measured at 300 K (RTP) (RTP = room temperature phase). Under RTP, compound **1** crystallizes in the non-centrosymmetric space group $Cmc2_1$ (orthorhombic system, point group $mm2$ with four symmetric elements (E, C_2, and $2\sigma_v$)) with cell parameters a = 9.1323(5) Å, b = 10.3481(6) Å, c = 14.8559(8) Å, $\alpha = \beta = \gamma$ = 90°, V = 1403.91(14) $Å^3$, Z = 4 (Table S1†). As shown in Fig. 2a, the asymmetric unit of compound **1** at RTP consists of a protonated $(C_8H_{14}NO)^+$ cation and a twisted $[FeCl_4]^-$ anionic tetrahedron, consistent with charge conservation, and double disorder of organic cations can be seen. The bond lengths and angles are shown in Tables S2 and S3.† The distance range of the Fe–Cl bond is 2.1746(18) Å–2.1954(10) Å, and the angle range of Fe–Cl–Fe is 107.68(7)°–113.20(10)°. From the packing structure along the b-axis, as shown in Fig. 2c, the disordered $(C_8H_{14}NO)^+$ organic cations and $[FeCl_4]^-$ inorganic anion tetrahedra are arranged alternately, forming a zero-dimensional framework that provides more freedom for the movement of organic cations, resulting in ferroelectric phase transitions. It is worth noting that in the molecule, organic cations are distributed in the upper left or upper right direction. This arrangement results in a net polarization along the c-axis. (Fig. 2b).[38]

Because the crystal quality of compound **1** is affected by high temperature, the diffraction data of a single crystal at high temperature are poor, and the complete crystal structure of compound **1** cannot be obtained. Fortunately, the reversible structural phase transition of compound **1** can be confirmed by thermostatic PXRD. At 298 K, according to the single crystal structure, the PXRD patterns were in good agreement with the simulated results (Fig. S3†), indicating a high purity of compound **1**. As shown in Fig. 3a, the diffraction peak of compound **1** does not change significantly when heated from 298 K to 338 K, indicating that the structure remains relatively

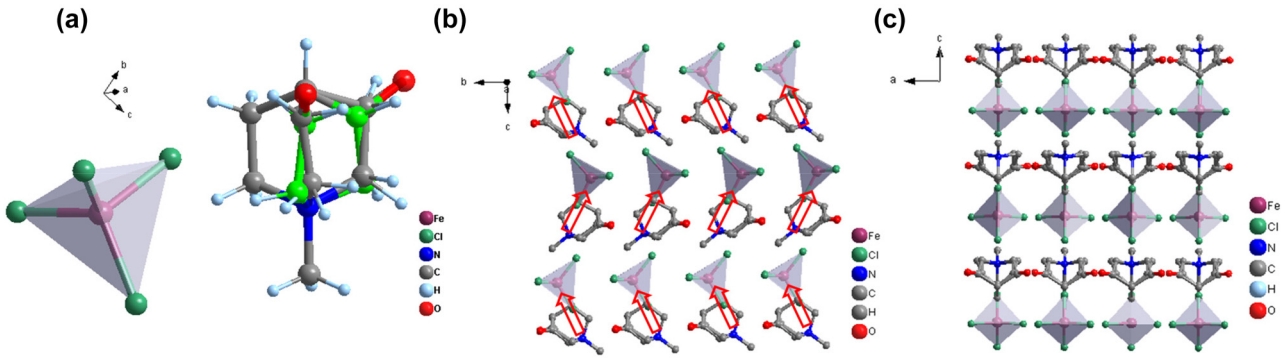

Fig. 2 The asymmetric unit of compound **1** (a) (the green atoms represent disordered carbon atoms). Packing view of **1** at 300 K viewed along the a-axis (b). The red arrows represent the direction of polarization. Packing view of **1** at 300 K viewed along the b-axis (c).

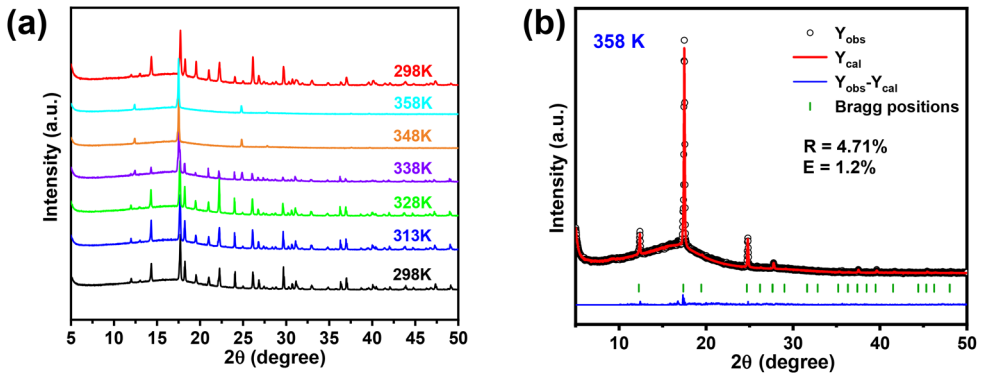

Fig. 3 Variable-temperature PXRD patterns of **1** (a). Structural refinement results of PXRD data for compound **1** at 358 K (HTP) (b).

stable over a wide temperature range below T_c. With the increase of temperature, the number of diffraction peaks at 348–358 K decreases obviously, indicating that the crystal structure changes from low symmetry to high symmetry. When the temperature was cooled down to 298 K, these reduced peaks reappeared and returned to the original state, indicating that compound **1** had undergone a reversible structural phase transition, which was consistent with the results of DSC tests. At the same time, Le Bail refinement was performed on PXRD data at HTP (HTP = high temperature phase) to further understand the structural information at high temperature (Fig. 3b). The PXRD data after Le Bail refinement at 358 K provide cell parameters of the high temperature phase: a = 10.1902 Å, b = 10.1902 Å, c = 3.3976 Å, $\alpha = \gamma = \beta = 90°$, V = 352.8 Å^3. Based on the related physical properties, it is speculated that the high temperature phase of compound **1** may adopt the 4/*mmm* point group, of which the most likely space group is *P*4/*mmm*. More specifically, this symmetry breaking occurs in the Aizu notation 4/*mmm*F*mm*2.

SHG response and ferroelectric properties

The second harmonic generation (SHG) method is the most direct method to detect the symmetry of crystals. The SHG signal is very sensitive to the transition from a non-centrosymmetric structure to a centrosymmetric structure, and the structural phase transition can be verified. Variable temperature SHG signal measurement is an effective method to detect the symmetry breaking of a crystal structure.[39,40] Compound **1** crystallizes in the polar non-centrosymmetric space group *Cmc*2$_1$. Therefore, the variation of SHG signal intensity with temperature was measured. As shown in Fig. 4a, below T_c, a clear SHG signal can be observed, and its strength is stable around 0.60 (a.u.). When the temperature rises to about 336 K (HTP), the SHG signal strength drops sharply to close to 0 (a.u.). The strong SHG intensities below T_c and zero SHG intensities above T_c indicate non-centrosymmetric and centrosymmetric phases, respectively, corresponding to the phase transition from the non-centrosymmetric space group *Cmc*2$_1$ in the low temperature phase to the central space group *P*4/*mmm* in the high temperature phase. At the same time, the trend of temperature-dependent SHG signal intensity confirms the first-order phase transition in compound **1**. Meanwhile, SHG intensity dependence on particle size was analyzed according to the Kurtz–Perry method; however, compound **1** did not display phase matching (Fig. 4b). This nonphase-matching behavior is well consistent with that reported by Kurtz and Perry and may be attributed to the value of $L/\hat{r}$ (where L represents the powder-layer thickness and $\hat{r}$ represents the average particle size).[41–43]

The symmetry breaking diagram of compound **1** is shown in Fig. 5; compound **1** clearly undergoes a paraelectric-to-ferroelectric phase transition belonging to the 4/*mmm*F*mm*2 type

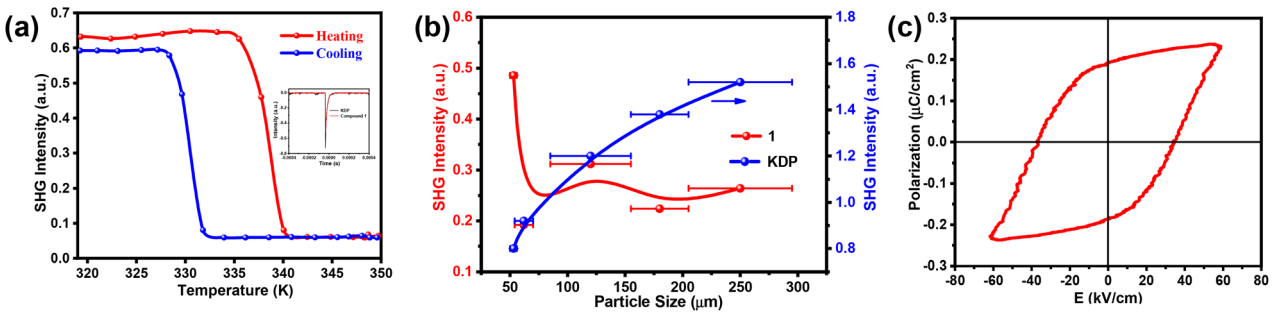

Fig. 4 Variable-temperature SHG signal of **1** (a). Dependence of the SHG intensity of **1** on the particle size at 1064 nm (KDP samples as references) (b). *P*–*E* hysteresis loop of **1** measured at room temperature (c).

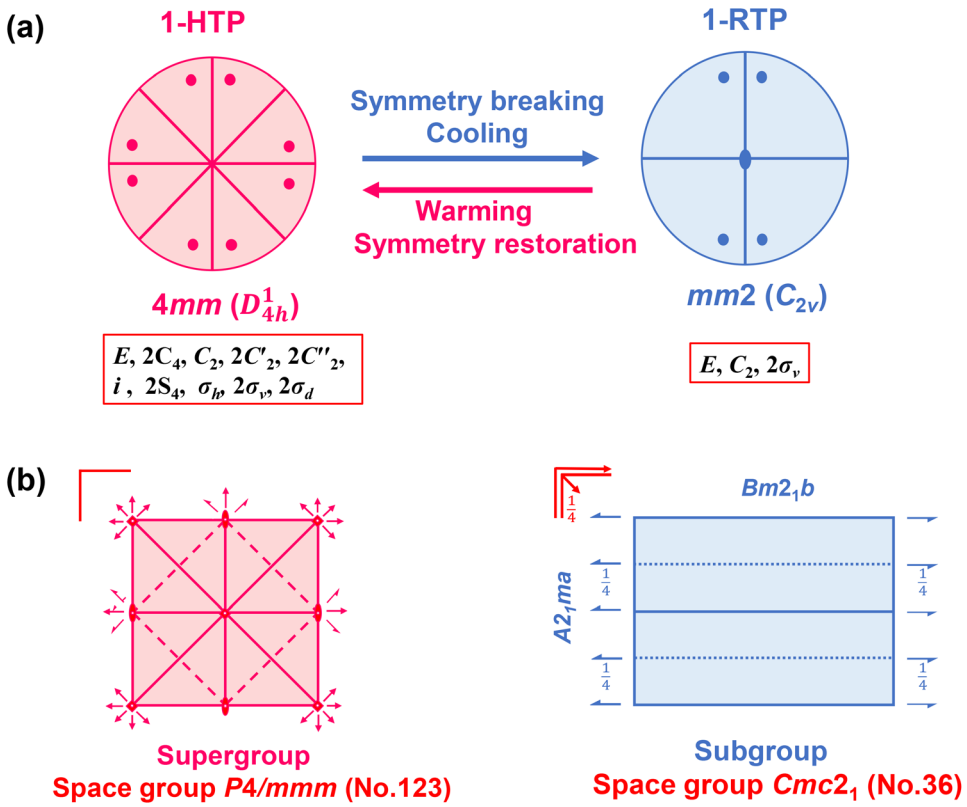

Fig. 5 The equatorial plane projection (a) and spatial symmetry operation diagram (b) of **1**-HTP and **1**-RTP.

according to the Aizu rule. The paraelectric point group 4/*mmm* and the ferroelectric point group *mm*2 have 16 and 4 symmetry elements, respectively, which reveals a multiaxial ferroelectric with 4 equivalent polarization directions, corresponding to 2 equivalent ferroelectric axes. Interestingly, most organic–inorganic hybrid ferroelectrics exhibit uniaxial ferroelectric properties. The multi-axis property of **1** will simplify the preparation of polycrystalline films.

The polarization electric (*P*–*E*) field hysteresis loop test provides direct evidence to prove whether the crystalline material has ferroelectric properties. In order to confirm the ferroelectric properties of compound **1**, the polarization electric (*P*–*E*) field hysteresis loop was measured. A well-shaped *P*–*E* hysteresis loop was obtained using the Sawyer–Tower circuit method (Fig. 4c), and the measured saturation polarization value (P_s) was about 0.24 μC cm^{-2}, which is much higher than that of molecular ferroelectrics [$(CH_3)_3NCH_2CHCH_2$][$FeCl_4$] (0.18 μC cm^{-2}),[7] (formamidine)$_3$[Bi_2I_9] (0.04 μC cm^{-2}),[44] and (tetramethyl-phosphonium)$_3$[Sb_2Cl_9] (0.05 μC cm^{-2}).[45] The spontaneous polarization of compound **1** is smaller than that of [$(CH_3)_4N$][$FeCl_4$] (3.3 μC cm^{-2}),[46] ($C_6H_5CH_2CH_2NH_3)_2$[CdI_4] (0.36 μC cm^{-2}),[22] and (DMA)$_4$[PbI_6] (0.36 μC cm^{-2}),[24] but its Curie temperature (T_c = 341.8 K) is much higher than theirs. Our subsequent work will focus on exploring molecular ferroelectrics with high phase transition temperature, large spontaneous polarization, and high piezoelectric properties.

To further confirm the ferroelectric behavior of compound **1**, its films were measured by piezoelectric response force (PFM) microscopy, which is the most powerful method for characterizing ferroelectric materials.[47] Vertical and lateral PFM imaging can detect the out-of-plane and in-plane components of polarization, respectively. Fig. 6a and b, respectively, show the lateral amplitude and phase diagrams of compound **1**, and Fig. 6c and d, respectively, show the corresponding vertical amplitude and phase diagrams at the same position. The lateral and vertical phase diagrams show distinct non-180° domains and are separated by domain walls, exhibiting a multi-axial property. At the same time, a typical butterfly loop (Fig. 6e) and a hysteresis loop (Fig. 6f) further confirm that compound **1** films have good ferroelectric switching properties.

The most essential characteristic of ferroelectrics is that they can realize spontaneous polarization under the action of an applied electric field. In order to verify the switchable spontaneous polarization of compound **1**, PFM tip polarization experiments were carried out to clearly show the domain switchable process in compound **1** thin films, with a selected region of 4 μm × 4 μm.[48] After +60 V tip bias is applied at the yellow point to polarize the film surface for 1 second, as shown in Fig. S5,† the polarization direction of the region marked with the yellow dashed ellipse is redirected (Fig. S5b†). Then, an opposite tip bias of −60 V is applied at the green dot for 1 second, and the direction of polarization of the region

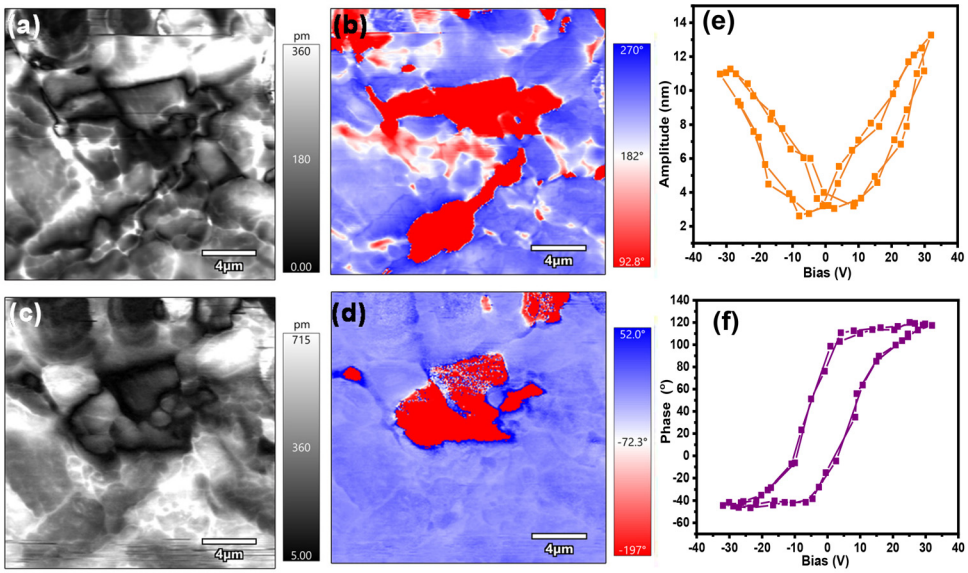

Fig. 6 The lateral and vertical PFM amplitude (a and c) and phase (b and d) mapping of compound **1**. An amplitude–voltage butterfly loop (e) and a phase–voltage hysteresis loop (f) of compound **1**.

marked with the green dashed ellipse is redirected (Fig. S5c†). These PFM measurements strongly demonstrated the presence of stable and switchable polarization in compound **1** films. The switchable spontaneous polarization makes it a potential storage material.

Conclusions

In conclusion, we have successfully synthesized and characterized a multifunctional organic–inorganic hybrid metal halide ferroelectric $(C_8H_{14}NO)[FeCl_4]$. By using single crystal structure measurement and variable temperature PXRD, it is revealed that the compound undergoes a reversible structural phase transition. Notably, it shows multiaxial ferroelectricity (Aizu notation: 4/*mmmFmm*2) and ferroelectric–paraelectric phase transition at 341.8 K. This discovery provides a new way to explore molecular ferroelectrics with multiaxial properties and high phase transition temperature, especially in electrical–thermal double switch and other applications.

Author contributions

Yun-Zhi Tang, Yu-Hui Tan and Fang-Xin Wang conceived the experiment and co-wrote the manuscript. Fang-Xin Wang, Hao Zhang and Yu-Kong Li performed the experiments. All the authors discussed the results.

Conflicts of interest

There are no conflicts to declare.

Acknowledgements

This work was supported by the National Natural Science Foundation of China (Grant no. 21761013, 21671086, 21461010, and 21471070) and the Science and Technology Bureau project of Ganzhou.

References

1 W. Zhang and R. G. Xiong, Ferroelectric metal-organic frameworks, *Chem. Rev.*, 2012, **112**, 1163–1195.
2 J. Li, Y. Liu, Y. Zhang, H. L. Cai and R. G. Xiong, Molecular ferroelectrics: where electronics meet biology, *Phys. Chem. Chem. Phys.*, 2013, **15**, 20786–20796.
3 J. C. Zhuang, W. J. Wei, N. Song, Y. Z. Tang, Y. H. Tan, D. C. Han and Y. K. Li, A Narrow Bandgap of 2D Ruddlesden-Popper Bilayer Perovskite with Giant Entropy Change and Photoluminescence, *Chem. – Eur. J.*, 2021, **27**, 15716–15721.
4 W. J. Xu, K. Romanyuk, J. M. G. Martinho, Y. Zeng, X. W. Zhang, A. Ushakov, V. Shur, W. X. Zhang, X. M. Chen, A. Kholkin and J. Rocha, Photoresponsive Organic-Inorganic Hybrid Ferroelectric Designed at the Molecular Level, *J. Am. Chem. Soc.*, 2020, **142**, 16990–16998.
5 H. Zhang, Y. H. Tan, Y. Z. Tang, X. W. Fan, X. L. Peng, R. R. Han, Y. K. Li and F. X. Wang, Two Manganese(II)-Based Hybrid Multifunctional Phase Transition Materials with Strong Photoluminescence, High Quantum Yield, and Switchable Dielectric Properties: $(C_6NH_{16})_2MnBr_4$and $(C_7NH_{18})_2MnBr_4$, *Inorg. Chem.*, 2022, **61**, 10454–10460.
6 T. T. Ying, H. J. Shi, S. P. Chen, Y. Z. Tang, Y. H. Tan, S. F. Wang, Z. Sun, F. X. Wang and M. Y. Wan, Large

Spontaneous Polarization Ferroelectric Property, Switchable Second-Harmonic Generation Responses, and Magnetism in an Fe-Based Compound, *Inorg. Chem.*, 2023, **62**, 6189–6195.

7 T. Ying, Y. Tan, Y. Tang, X. Fan, F. Wang, M. Wan, J. Liao and Y. Huang, High-Tc Quadratic Nonlinear Optical and Dielectric Switchings in Fe-Based Plastic Crystalline Ferroelectric, *Inorg. Chem.*, 2022, **61**, 20608–20615.

8 Z. Yang, S. Jiao, Z. Tang, X. Sun, D. Li, P. Chen, Y. Lu, W. Zhang, H. Cai and X. Wu, Lead-Free Hybrid Organic-Inorganic Ferroelectric: (3,3-Difluoropyrrolidinium)$_2$ZnCl$_4$.H$_2$O, *Inorg. Chem.*, 2023, **62**, 4181–4187.

9 X. L. Xu, L. B. Xiao, J. Zhao, B. K. Pan, J. Li, W. Q. Liao, R. G. Xiong and G. F. Zou, Molecular Ferroelectrics-Driven High-Performance Perovskite Solar Cells, *Angew. Chem., Int. Ed.*, 2020, **59**, 19974–19982.

10 Y.-K. Li, Y.-H. Tan, Y.-Z. Tang, X.-W. Fan, S.-F. Wang, T.-T. Ying and H. Zhang, Unusual high-temperature host–guest inclusion compound-based ferroelectrics with nonlinear optical switching and large spontaneous polarization behaviours, *Inorg. Chem. Front.*, 2022, **9**, 3702–3708.

11 Y. K. Li, Y. Y. Lai, T. T. Ying, D. C. Han, Y. H. Tan, Y. Z. Tang, P. K. Du and H. Zhang, A multifunctional molecular ferroelectric with chiral features, a high Curie temperature, large spontaneous polarization and photoluminescence: $(C_9H_{14}N)_2CdBr_4$, *Chem. Sci.*, 2021, **12**, 13061–13067.

12 Y. K. Li, Y. Liu, Y. Z. Tang, W. J. Wei, N. Song, P. K. Du and D. C. Han, Syntheses, Crystal Structures, SHG Response and Purple Luminescent Property of Tetra(isothiocyanate) Mn(II) and Substituted Benzyl Triphenylphosphonium Cations, *Chin. J. Struct. Chem.*, 2021, **6**, 739–745.

13 Y. Wang, C. Shi and X.-B. Han, Organic–inorganic hybrid [H$_2$mdap][BiCl$_5$] showing an above-room-temperature ferroelectric transition with combined order–disorder and displacive origins, *Polyhedron*, 2017, **133**, 132–136.

14 C. Shi, L. Ye, Z. X. Gong, J. J. Ma, Q. W. Wang, J. Y. Jiang, M. M. Hua, C. F. Wang, H. Yu, Y. Zhang and H. Y. Ye, Two-Dimensional Organic-Inorganic Hybrid Rare-Earth Double Perovskite Ferroelectrics, *J. Am. Chem. Soc.*, 2020, **142**, 545–551.

15 P. Xu, H. Ye, Y. Yao, T. Zhu and J. Luo, Lead-free Double Perovskite Semiconductor with Rigid Spacer-Induced High-Tc Dielectric Switch Features, *Chem. – Eur. J.*, 2023, **29**, e202300667.

16 L. Hua, J. Wang, Y. Liu, W. Guo, Y. Ma, H. Xu, S. Han, J. Luo and Z. Sun, Improper High-Tc Perovskite Ferroelectric with Dielectric Bistability Enables Broadband Ultraviolet-to-Infrared Photopyroelectric Effects, *Adv. Sci.*, 2023, **10**, e2301064.

17 L. Chen, W. Q. Liao, Y. Ai, J. Li, S. Deng, Y. Hou and Y. Y. Tang, Precise Molecular Design Toward Organic-Inorganic Zinc Chloride ABX(3) Ferroelectrics, *J. Am. Chem. Soc.*, 2020, **142**, 6236–6243.

18 H. Y. Zhang, X. J. Song, H. Cheng, Y. L. Zeng, Y. Zhang, P. F. Li, W. Q. Liao and R. G. Xiong, A Three-Dimensional Lead Halide Perovskite-Related Ferroelectric, *J. Am. Chem. Soc.*, 2020, **142**, 4604–4608.

19 Y.-P. Gong, X.-X. Chen, G.-Z. Huang, W.-X. Zhang and X.-M. Chen, Ferroelasticity, thermochromism, semi-conductivity, and ferromagnetism in a new layered perovskite: (4-fluorophenethylaminium)$_2$[CuCl$_4$], *J. Mater. Chem. C*, 2022, **10**, 5482–5488.

20 D. C. Han, Y. H. Tan, W. C. Wu, Y. K. Li, Y. Z. Tang, J. C. Zhuang, T. T. Ying and H. Zhang, High-Temperature Phase Transition Containing Switchable Dielectric Behavior, Long Fluorescence Lifetime, and Distinct Photoluminescence Changes in a 2D Hybrid CuBr$_4$ Perovskite, *Inorg. Chem.*, 2021, **60**, 18918–18923.

21 H. Zhou, K. Yang, Y. Liu, Y. Tang, W. Wei, Q. Shu, J. Zhao and Y. Tan, In situ [2 + 3] cycloaddition synthesis, crystal structures, strong SHG responses and fluorescence properties of three novel Zn coordination polymers, *Chin. Chem. Lett.*, 2020, **31**, 841–845.

22 B. Huang, L. Y. Sun, S. S. Wang, J. Y. Zhang, C. M. Ji, J. H. Luo, W. X. Zhang and X. M. Chen, A near-room-temperature organic-inorganic hybrid ferroelectric: [C$_6$H$_5$CH$_2$CH$_2$NH$_3$]$_2$[CdI$_4$], *ChemComm*, 2017, **53**, 5764–5766.

23 Z. Gao, Y. Wu, Z. Tang, X. Sun, Z. Yang, H.-L. Cai and X. S. Wu, Ferroelectricity of trimethylammonium bromide below room temperature, *J. Mater. Chem. C*, 2020, **8**, 5868–5872.

24 Y. Wang, Z. Tang, C. Liu, J. Jiang, W. Liu, B. Zhang, K. Gao, H.-L. Cai and X. Wu, Room temperature ferroelectricity and blue photoluminescence in zero dimensional organic lead iodine perovskites, *J. Mater. Chem. C*, 2021, **9**, 223–227.

25 D. W. Fu, H. L. Cai, S. H. Li, Q. Ye, L. Zhou, W. Zhang, Y. Zhang, F. Deng and R. G. Xiong, 4-Methoxyanilinium perrhenate 18-crown-6: a new ferroelectric with order originating in swinglike motion slowing down, *Phys. Rev. Lett.*, 2013, **110**, 257601.

26 H. Y. Ye, Q. Zhou, X. Niu, W. Q. Liao, D. W. Fu, Y. Zhang, Y. M. You, J. Wang, Z. N. Chen and R. G. Xiong, High-Temperature Ferroelectricity and Photoluminescence in a Hybrid Organic-Inorganic Compound: (3-Pyrrolinium)MnCl$_3$, *J. Am. Chem. Soc.*, 2015, **137**, 13148–13154.

27 C.-F. Wang, N. Wang, L. Liu, L.-p. Miao, H.-Y. Ye, Y. Zhang and C. Shi, Enantiomeric hybrid high-temperature multiaxial ferroelectrics with a narrow bandgap and high piezoelectricity, *Chin. Chem. Lett.*, 2023, **34**, e108051.

28 H. Y. Zhang, Y. Y. Tang, P. P. Shi and R. G. Xiong, Toward the Targeted Design of Molecular Ferroelectrics: Modifying Molecular Symmetries and Homochirality, *Acc. Chem. Res.*, 2019, **52**, 1928–1938.

29 C. K. Yang, Y. T. Ding, J. Wang, Y. Rao, W. Q. Liao, Y. F. Xie, W. N. Zou and R. G. Xiong, Directional Intermolecular Interactions for Precise Molecular Design of a High-Tc Multiaxial Molecular Ferroelectric, *J. Am. Chem. Soc.*, 2019, **141**, 1781–1787.

30 Y. Zhang, W. Zhang, S. H. Li, Q. Ye, H. L. Cai, F. Deng, R. G. Xiong and S. D. Huang, Ferroelectricity induced by ordering of twisting motion in a molecular rotor, *J. Am. Chem. Soc.*, 2012, **134**, 11044–11049.

31 P. González-Izquierdo, O. Fabelo, L. Cañadillas-Delgado, G. Beobide, O. Vallcorba, J. Salgado-Beceiro, M. Sánchez-Andújar, C. Martin, J. Ruiz-Fuentes, J. E. García, M. T. Fernández-Díaz and I. de Pedro, ((R)-(-)-3-Hydroxyquinuclidium)[$FeCl_4$]; a plastic hybrid compound with chirality, ferroelectricity and long range magnetic ordering, *J. Mater. Chem. C*, 2021, **9**, 4453–4465.

32 Y. M. You, H. Y. Ye, Y. Zhang, Q. H. Zhou, X. H. Niu, J. L. Wang, P. F. Li, D. W. Fu, Z. M. Wang, S. Gao, K. L. Yang, J. M. Liu, J. Y. Li, Y. F. Yan and R. G. Xiong, An organic-inorganic perovskite ferroelectric with large piezoelectric response, *Science*, 2017, **357**, 306–309.

33 X. N. Hua, W. Q. Liao, Y. Y. Tang, P. F. Li, P. P. Shi, D. Zhao and R. G. Xiong, A Room-Temperature Hybrid Lead Iodide Perovskite Ferroelectric, *J. Am. Chem. Soc.*, 2018, **140**, 12296–12302.

34 W. J. Xu, P. F. Li, Y. Y. Tang, W. X. Zhang, R. G. Xiong and X. M. Chen, A Molecular Perovskite with Switchable Coordination Bonds for High-Temperature Multiaxial Ferroelectrics, *J. Am. Chem. Soc.*, 2017, **139**, 6369–6375.

35 J. C. Zhuang, Y. H. Zhang, N. Song, Y. H. Tan, Y. Z. Tang, Y. L. Huang, H. Zhang and Y. K. Li, Neutral 1D Perovskite-Type ABX_3 Phase Transition Material with a Narrowband Emission and Semiconductor Property, *Chem. – Asian J.*, 2022, **17**, e202101134.

36 Y. Ai, P. F. Li, M. J. Yang, Y. Q. Xu, M. Z. Li and R. G. Xiong, An organic plastic ferroelectric with high Curie point, *Chem. Sci.*, 2022, **13**, 748–753.

37 J. Li, C. Xu, W.-Y. Zhang, P.-P. Shi, Q. Ye and D.-W. Fu, Smart and efficient opto-electronic dual response material based on two-dimensional perovskite crystal/thin film, *J. Mater. Chem. C*, 2020, **8**, 1953–1961.

38 T.-T. Ying, Y.-Z. Tang, Y.-H. Tan, Y.-R. Zhao, J.-Y. Wang, M.-Y. Wan, F. X. Wang, X. W. Fan and Y. K. Li, Organic Single-Component Enantiomers with High Phase Transition Temperatures and Dielectric Switching Properties, *Cryst. Growth Des.*, 2022, **22**, 7501–7507.

39 Y. Zheng, J. Xu and X. H. Bu, 1D Chiral Lead Halide Perovskites with Superior Second–Order Optical Nonlinearity, *Adv. Opt. Mater.*, 2022, **10**, e2101545.

40 B. Li, Y. Yu, M. Xin, J. Xu, T. Zhao, H. Kang, G. Xing, P. Zhao, T. Zhang and S. Jiang, Second-order nonlinear optical properties of copper-based hybrid organic-inorganic perovskites induced by chiral amines, *Nanoscale*, 2023, **15**, 1595–1601.

41 B. Zhao, Y. Yang, S. Zhao, Y. Shen, X. Li, L. Li, C. Ji, Z. Lin and J. Luo, A new phase-matchable nonlinear optical silicate: $Rb_2ZnSi_3O_8$, *J. Mater. Chem. C*, 2017, **5**, 11025–11029.

42 S. K. Kurtz and T. T. Perry, A Powder Technique for the Evaluation of Nonlinear Optical Materials, *J. Appl. Phys.*, 1968, **39**, 3798–3813.

43 W.-J. Wei, H.-Q. Gao, Y. Yang, M. Fang, X.-D. Wang, X. Chen, W.-L. Qin, G.-Q. Chen, R.-X. Li, Y.-Z. Tang and Y. Wei, Zero-Dimensional Molecular Ferroelectrics with Significant Nonlinear Effect and Giant Entropy, *Chem. Mater.*, 2022, **34**, 6323–6330.

44 P. Szklarz, A. Gągor, R. Jakubas, P. Zieliński, A. Piecha-Bisiorek, J. Cichos, M. Karbowiak, G. Bator and A. Ciżman, Lead-free hybrid ferroelectric material based on formamidine: $[NH_2CHNH_2]_3Bi_2I_9$, *J. Mater. Chem. C*, 2019, **7**, 3003–3014.

45 M. Wojciechowska, A. Gągor, A. Piecha-Bisiorek, R. Jakubas, A. Ciżman, J. K. Zaręba, M. Nyk, P. Zieliński, W. Medycki and A. Bil, Ferroelectricity and Ferroelasticity in Organic Inorganic Hybrid (Pyrrolidinium)$_3$[Sb_2Cl_9], *Chem. Mater.*, 2018, **30**, 4597–4608.

46 J. Harada, N. Yoneyama, S. Yokokura, Y. Takahashi, A. Miura, N. Kitamura and T. Inabe, Ferroelectricity and Piezoelectricity in Free-Standing Polycrystalline Films of Plastic Crystals, *J. Am. Chem. Soc.*, 2018, **140**, 346–354.

47 X. G. Chen, Y. Y. Tang, H. P. Lv, X. J. Song, H. Peng, H. Yu, W. Q. Liao, Y. M. You and R. G. Xiong, Remarkable Enhancement of Piezoelectric Performance by Heavy Halogen Substitution in Hybrid Perovskite Ferroelectrics, *J. Am. Chem. Soc.*, 2023, **145**, 1936–1944.

48 Z. H. Wei, Z. T. Jiang, X. X. Zhang, M. L. Li, Y. Y. Tang, X. G. Chen, H. Cai and R. G. Xiong, Rational Design of Ceramic-Like Molecular Ferroelectric by Quasi-Spherical Theory, *J. Am. Chem. Soc.*, 2020, **142**, 1995–2000.